Theoretical study of the photocurrent in transition-metal dichalcogenide materials

Hyun C. Lee*

Department of Physics and Basic Science Research Institute, Sogang University, Seoul, Korea

(Received 15 March 2017; revised manuscript received 17 May 2017; published 2 June 2017)

Motivated by photocurrent spectroscopy experiments with MoS_2, the direct band-to-band transition contribution to the photocurrent of transition-metal dichalcogenides is computed starting from the microscopic Hamiltonian in the Keldysh-Schwinger formalism. It turns out that the band tilting induced by source to drain voltage is necessary for a nonvanishing photocurrent. The photon energy dependence of the normalized photocurrent is found to be consistent with experimental data. For circular polarization the helicity-dependent component of the photocurrent perpendicular to the band-tilting direction is predicted, which essentially originates from the valley Hall effect.

DOI: 10.1103/PhysRevB.95.245102

I. INTRODUCTION

Atomically thin two-dimensional (2D) crystals [1,2] are a very unique class of materials which are currently under intensive study, and they also provide a new arena for next-generation electronic devices [3,4].

Among these, graphene was studied in detail formerly [5]. Graphene has a honeycomb lattice structure which can be regarded as a hexagonal lattice with two basis atoms in a unit cell. The key feature of the energy band of graphene is the existence of two gapless Dirac cones at the corners (K and K') of the Brillouin zone (BZ), and this structure at K and K' constitutes the so-called *valley* degrees of freedom. In spite of many remarkable physical properties, the gapless band structure (semimetallicity) of graphene often poses limitations from the viewpoint of conventional semiconductor electronic devices. Furthermore, the spin-orbit coupling of graphene is very small, making its application to spintronics very difficult.

Layered transition-metal dichalcogenides (TMDCs) is a class of materials which can be tailored into a monolayer with a band gap [1], lifting the limitations associated with the semimetallicity of graphene. The chemical formula of TMDCs takes the form MX_2, where M is a transition-metal element such as Mo or W and X is a chalcogenide element such as S, Se, or Te. TMDCs have the same hexagonal Bravais lattice as graphene; therefore, they inherit the same valley degrees of freedom with the sublattice degrees of freedom of graphene replaced by the species of d orbitals of M of TMDCs. Also, the strong spin-orbit coupling stemming from the d orbital of M, being combined with the broken inversion symmetry of the monolayer, leads to a significant spin-orbit splitting in the valence band [6]. This is an important feature relevant to spintronics applications.

The valley degrees of freedom is an internal quantum number and it can play a role similar to that of real spin [7]. For layered TMDCs, the layer index can be also regarded as another sort of internal quantum number. These internal quantum numbers are often called *pseudospin*, and they can give rise to diverse physical phenomena such as the *valley Hall effect* [7]. We will see below that this valley Hall effect also manifests itself in our study of photocurrents [see Eq. (63)].

As the number of layers of a TMDC decreases to 1, the band structure is found to evolve from an indirect gap to a direct gap at K and K' [8,9]. The direct-gap (in the visible range) nature of monolayer TMDCs is very crucial in understanding its optical properties. The optical absorption experiments on TMDCs clearly reveal the exciton states with very large binding energies of the order of a few hundred meV [9], which are consistent with theoretical calculations [10,11]. These large binding energies are attributed to the insufficient screening in 2-dimensional monolayers compared to bulk 3-dimensional material [12].

The aforementioned excitons are also clearly observable in the photocurrent spectroscopy of MoS_2 (see Fig. 2 of [13]). The A peak at 1.9 eV and B peak at 2.1 eV come from the optical transitions from spin-orbit split valence bands to the exciton state. The experimentally obtained band gap is about 2.5 eV, so the photocurrent experiment implies a very large exciton binding energy around 600 meV. A broad and much stronger C peak at 2.9 eV above the band gap is attributed to the excitons associated with the Van Hove singularity (band nesting) near the Γ point, where the p orbitals of disulfide also contribute [10,13]. However, this C peak also includes the contribution from the direct band-to-band transition at the K and K' points, which cannot be easily distinguished from the exciton contributions near the Γ point [13]. In passing, we note that the experiment of [13] has been performed in the presence of source to drain bias voltage (greater than 3 V), which causes tilting of the energy bands.

In order for the exciton states to contribute to the photocurrent, the bound electron-hole pairs must be unbound. In Ref. [13], it is argued that the unbinding of electron-hole pairs is made possible due to the strong electric field between MoS_2 and metallic contacts. Now it is known that the exciton binding energy can be affected by carrier scattering via screening [14]. Then it is plausible that the strong electric field which can break up the tightly bound electron-hole pair will also modify screening effects, which are regarded as being responsible for very large binding energies. Evidently, the full theoretical study of the roles of the above electric field on exciton states would be rather complicated.

In this paper we focus on the direct band-to-band transition contribution to the photocurrent leaving aside the complex problem of the exciton contribution to the photocurrent above the band gap. There are two reasons for this. First we know

*hyunlee@sogang.ac.kr

that the direct band-to-band transition does contribute to the photocurrent above the band gap. Thus, before trying to interpret the C peak in terms of excitons coming from the Van Hove singularity, it is necessary to assess the direct band-to-band transition contribution to the C peak. Second, from a practical point of view, the C peak is much stronger than the A and B peaks, so is more relevant for applications.

We compute the direct band-to-band transition contribution to the photocurrent starting from the microscopic Hamiltonian, and see how it compares with the experiment of [13]. It turns out the nonvanishing contribution is possible only in the presence of source to drain bias voltage. This bias voltage is incorporated in the form of the band-tilting term into the microscopic Hamiltonian, and we compute the photocurrent explicitly for arbitrary incidence angle of photons and for both linear and circular polarizations. The momentum relaxation mechanism is also included explicitly via the random potential scattering Hamiltonian rather than being introduced by hand.

The photocurrent should be of the (at least) second order in the vector potential of incoming photon (see Secs. II A and II C). In other words, it is beyond the linear response regime. The photocurrent is determined by the change of charge carrier densities due to photons and by the scattering of these charge carriers. In the Keldysh-Schwinger (KS) formalism [15–17], the distribution and the scattering of charge carriers can be treated in a unified way, allowing us to compute the photocurrent directly through the Feynman diagram method. For the above two reasons, we adopt the KS formalism as a calculational tool in this paper.

The main results of this paper are Eqs. (59), (60), (62), and (63), which can be summarized as follows: (1) The direct band-to-band transition contributes to the photocurrent only in the presence of source to drain bias voltage. (2) The photon energy dependence of the (normalized) photocurrent is given by $(\omega_{\rm p}-\Delta)/\omega_{\rm p}^{n}$ $(n=6 \text{ or } 8)$, where $\omega_{\rm p}$ is the incoming photon energy and Δ is the band gap. This $\omega_{\rm p}$ dependence is consistent with experimental data around the C peak for the experimental value of the band gap. (3) For circular polarization, there exists a helicity-dependent component of photocurrent perpendicular to the band-tilting direction, which is in accordance with the valley Hall effect. (4) The photocurrents have a distinctive angle dependence which is determined by photon polarization and photon incidence angle.

This paper is organized as follows: We set up the Hamiltonians and KS formalism for our problem in Sec. II along with some remarks. The self-energy of the KS Green's function and the photocurrent is computed in Sec. III, and the results are presented in Sec. IV with discussion. We conclude the paper in Sec. V.

II. SETUP

A. Preliminary remarks

In this subsection a few remarks are made which aim at justifying the approach taken in this paper. First we note that the experiment of [13] has been performed under the conditions of very low laser intensity ($\leqslant 30\,\mathrm{pW}/\mu\mathrm{m}^2$) and low temperature (77 K). These experimental conditions allow one to exclude artifacts such as photo-thermoelectric effects [13]. We assume the case of intrinsic TMDCs, so that the electron carrier density n_e is the same as the hole carrier density n_h.

In general, the rate of the change of charge carrier density is determined by the generation rate R_g and recombination rate R_r [18]:

$$\frac{dn_e}{dt}=R_g-R_r. \tag{1}$$

The charge carriers can be generated by photon excitation (laser) and by thermal excitation; then the experimental conditions of [13] imply very small charge carrier density. The charge carrier density decreases by the recombination of electron and hole charge carriers. There are three main mechanisms of the recombination processes: band-to-band recombination, the Shockley-Read-Hall trap mechanism, and Auger processes [18]. The band-to-band recombination rate for direct band gap material is proportional to the product of electron and hole carrier densities, so that it will be much smaller than the generation rate for our case. Shockley-Read-Hall trap recombinations involve midgap impurity states and trap states near the interface, and their rate is proportional to carrier density. Since the experiment of [13] has been performed for a sample in a suspended state, we can presume that the trap mechanisms will be of minor effect. Finally, the Auger process is known to be important only for very large carrier density [18], which is not the case for the experiment of [13].

In summary, at least for the experimental conditions we are considering, we can neglect all the recombination processes. By considering the zero-temperature limit, we can also eliminate the carrier generation by thermal excitation; then the photon excitation will be the only mechanism for the carrier generation, which can be described by the second-order process in the photon vector potential (transition amplitude squared, the Born approximation). Of course, this does not mean the charge carrier density will increase with time indefinitely. Eventually, the charge carriers will reach electrodes and recombine in the voltage source.

If the recombination processes were not negligible, we would have to solve Eq. (1) self-consistently, which will involve higher-order terms in photon vector potentials. However, in our case the direct second-order perturbation in photon vector potential will suffice.

B. Hamiltonians

In this subsection we set up four Hamiltonians: band, band tilting, electron-photon interaction, and random potential scattering.

The space group of monolayer MoS_2 is D_{3h}^{1} which is one of the space groups of the hexagonal lattice [6]. The wave vector group at $K, K'=-K$ is C_{3h}. The minimal two-band Hamiltonian compatible with the symmetry group of the wave vector in the $k\cdot p$ approximation is given by [6] (mostly the $\hbar=1$ convention will be used in this paper)

$$\widehat{\mathsf{h}}_{(0)}=t_{\rm hop}a(k_x\hat{\tau}_z\hat{\sigma}_x+k_y\hat{\sigma}_y)+\frac{\Delta}{2}\hat{\sigma}_z-\lambda\hat{s}_z\hat{\tau}_z\left(\frac{\hat{\sigma}_z-1}{2}\right), \tag{2}$$

where $\hat{s}_i,\hat{\tau}_i,\hat{\sigma}_i$ $(i=x,y,z)$ are Pauli matrices acting on the spin, valley, and orbital space, respectively. The orbital space

is spanned by linear combinations of d orbitals of transition-metal element M. The values of the parameters for MoS_2 obtained from the first-principles band structure calculations are $a = 3.193$ Å (lattice spacing), $t_{\rm hop} = 1.10$ eV (hopping amplitude), $\Delta = 1.66$ eV (band gap), and $2\lambda = 0.15$ eV (spin-orbit splitting of the valence band) [6]. The spin-orbit splitting of the conduction band is neglected. We note that the photocurrent spectroscopy experiment [13] gives the value of gap $\Delta \sim 2.4$ eV. From now on, we will take MoS_2 as a prototype example of a TMDC to set various energy scales.

The product of Pauli matrices of different species in Eq. (2) should be understood in the sense of a tensor product, namely $\hat{\tau}_z\hat{\sigma}_x \equiv \hat{\tau}_z \otimes \hat{\sigma}_x$. The tensor product symbol and the identity matrices may not be displayed explicitly for the brevity of notations.

Note that the specific choice of x and y axes is implied in Eq. (2) by the placement of $\hat{\tau}_z$ along the x direction. From now on, $s,\eta = \pm 1$ denote the eigenvalues of $\hat{s}_z$ and $\hat{\tau}_z$, respectively. The energy eigenvalues of the Hamiltonian Eq. (2) are (+: conduction band, −: valence band)

$$E^{(0)}_{\pm}(\mathbf{k}) = \pm\sqrt{(\Delta'_{s\eta}/2)^2 + v^2k^2} + \frac{s\eta\lambda}{2}, \tag{3}$$

where $k^2 = k_x^2 + k_y^2$, $v \equiv t_{\rm hop}a$, and

$$\Delta'_{s\eta} = \Delta - s\eta\lambda. \tag{4}$$

Since the energy gap Δ is larger than the bandwidth ($\approx vk_{\rm max}$) (which is, in turn, larger than the spin-orbit splitting), Eq. (3) can be approximated by

$$E^{(0)}_{+}(\mathbf{k}) \approx \frac{\Delta}{2} + \frac{v^2k^2}{\Delta}, \quad E^{(0)}_{-}(\mathbf{k}) \approx -\frac{\Delta}{2} - \frac{v^2k^2}{\Delta} + s\eta\lambda. \tag{5}$$

The band-tilting Hamiltonian coming from source-drain bias voltage can be obtained in the following way. Clearly, the source-drain bias voltage can be described by a constant uniform electric field, which can be expressed by the scalar potential, $-\vec{E}_{\rm tilt}\cdot\vec{r}$. The detailed lattice structure is irrelevant for representing a macroscopic uniform electric field, and this implies that the representation of the band-tilting Hamiltonian should be independent of valley and orbital degrees of freedom (spin independence is, of course, obvious). Thus, the band-tilting Hamiltonian should be proportional to the identity matrix in spin, valley, and orbital space:

$$\widehat{\mathsf{h}}_{\rm tilt} = (e\vec{E}_{\rm tilt}\cdot\vec{r})\, \mathrm{I}^s_2 \otimes \mathrm{I}^\tau_2 \otimes \mathrm{I}^\sigma_2, \tag{6}$$

where the 2×2 identity matrices acting on the spin, valley, and orbital spaces have been indicated for clarity. Let $\vec{\ell}_t = (\cos\phi_t, \sin\phi_t)$ be the unit vector along $\vec{E}_{\rm tilt}$. The band tilting is known to exist in Weyl semimetals due to reduced symmetry [19], and it plays an important role in photocurrent [20]. We also note that the band-tilting term originates from the scalar potential, so it does not couple to the electric current. This means that the band-tilting Hamiltonian does not contribute to the electric current operator. The band-tilting Hamiltonian [Eq. (6)] will be treated perturbatively. It will turn out that the nonvanishing photocurrent will appear in the first (not zeroth) order perturbation.

Next we consider the interaction of the TMDC with photons (Zeeman coupling to the vector potential is ignored):

$$\mathsf{h}_{\rm e-ph} = -\frac{1}{c}\sum_{\mathbf{q}} \vec{J}(\mathbf{q})\cdot\vec{A}(-\mathbf{q}), \tag{7}$$

where $\vec{A}(-\mathbf{q})$ is the vector potential of the photon with momentum $-\mathbf{q}$, which is negligible in our case of optical transition. $\vec{J}(\mathbf{q})$ is the current density operator with momentum $\mathbf{q}$. Recalling that the band-tilting Hamiltonian does not contribute to the current operator, we find ($\hat{\mathbf{x}}$, $\hat{\mathbf{y}}$ denote the unit vector along the x and y axes, respectively)

$$\vec{J}(\mathbf{q}=0) = (-e)\frac{\partial \mathsf{h}_{(0)}(\mathbf{k})}{\partial \mathbf{k}} = (-e)v(\widehat{\mathsf{M}}_x\hat{\mathbf{x}} + \widehat{\mathsf{M}}_y\hat{\mathbf{y}}), \tag{8}$$

where $\widehat{\mathsf{M}}_{x,y}$ are 8×8 matrices defined by

$$\widehat{\mathsf{M}}_x = \mathrm{I}^s_2 \otimes \hat{\tau}_z \otimes \hat{\sigma}_x, \quad \widehat{\mathsf{M}}_y = \mathrm{I}^s_2 \otimes \mathrm{I}^\tau_2 \otimes \hat{\sigma}_y. \tag{9}$$

For clarity all relevant matrices are displayed explicitly.

Now let us specify the polarizations of incoming photons. We will consider the general case of an obliquely incident photon. Furthermore, we should allow arbitrary azimuth angle of the photon in the x-y plane since the specific choice of $\hat{\mathbf{x}}$,$\hat{\mathbf{y}}$ axes has already been made by Eq. (2). The momentum of incoming photon $\mathbf{k}_{\rm p}$ is taken to be

$$\begin{aligned}\mathbf{k}_{\rm p} &= |\mathbf{k}_{\rm p}|(-\sin\theta_{\rm p}\sin\phi_{\rm p}\widehat{\mathbf{x}} + \sin\theta_{\rm p}\cos\phi_{\rm p}\widehat{\mathbf{y}} - \cos\theta_{\rm p}\widehat{\mathbf{z}}) \\ &= |\mathbf{k}_{\rm p}|\,\widehat{\mathbf{k}}_{\rm p}.\end{aligned} \tag{10}$$

The $\theta_{\rm p}$ is the usual polar angle for the photon momentum coming from above, and $\phi_{\rm p}$ is the azimuth angle of the photon measured from the y axis counterclockwise.

S polarization is a linear polarization orthogonal to the $\widehat{\mathbf{k}}_{\rm p}$-$\widehat{\mathbf{z}}$ plane:

$$\widehat{\mathbf{e}}_2 = \cos\phi_{\rm p}\,\widehat{\mathbf{x}} + \sin\phi_{\rm p}\,\widehat{\mathbf{y}}. \tag{11}$$

The P polarization lies in the $\widehat{\mathbf{k}}_{\rm p}$-$\widehat{\mathbf{z}}$ plane, and it is also orthogonal to S polarization:

$$\widehat{\mathbf{e}}_1 = -\widehat{\mathbf{x}}\cos\theta_{\rm p}\sin\phi_{\rm p} + \widehat{\mathbf{y}}\cos\theta_{\rm p}\cos\phi_{\rm p} + \widehat{\mathbf{z}}\sin\theta_{\rm p}. \tag{12}$$

Then a general *linear* polarization state can be represented as

$$\widehat{\mathbf{e}}_{\mathbf{k}_{\rm p}} = \cos\varphi\,\widehat{\mathbf{e}}_1 + \sin\varphi\,\widehat{\mathbf{e}}_2, \tag{13}$$

and the corresponding vector potential (a certain profile function characterizing laser beam size is implicitly assumed) is given by

$$\vec{A}_{\rm linear}(\mathbf{r},t) = A_0\,\widehat{\mathbf{e}}_{\mathbf{k}_{\rm p}}\cos(\mathbf{k}_{\rm p}\cdot\mathbf{r} - \omega_{\rm p}t), \tag{14}$$

where $\omega_{\rm p} = |\mathbf{k}_{\rm p}|c > 0$, and A_0 is real. A factor like e^{0^+t} is implicitly assumed in Eq. (14) to ensure slow turning on of interaction, and 0^+ denotes an infinitesimally small positive quantity.

The *circular* polarization is represented by

$$\widehat{\mathbf{e}}_{\pm} = \frac{\widehat{\mathbf{e}}_1 \pm i\,\widehat{\mathbf{e}}_2}{\sqrt{2}}, \tag{15}$$

where the plus (minus) sign corresponds to the left (right) circularly polarized state with the helicity $\zeta = +1$ (-1). The

vector potential of the circularly polarized photon is given by (A_0 is real)

$$\vec{A}_{\pm}(\mathbf{r},t) = A_0[\hat{\mathbf{e}}_1 \cos(\mathbf{k}_\mathrm{p}\cdot\mathbf{r}-\omega_\mathrm{p}t) \mp \hat{\mathbf{e}}_2 \sin(\mathbf{k}_\mathrm{p}\cdot\mathbf{r}-\omega_\mathrm{p}t)]. \tag{16}$$

Both Eq. (14) and Eq. (16) contain the positive and the negative frequency component. In this paper, we will compute the electron current in the conduction band excited by the absorption of the photon, so only the negative frequency component needs to be included. The positive frequency component will contribute to the hole current, and in the leading order approximation of small spin-orbit coupling, the hole current contribution will be identical to that of the electron current. For this reason, we consider only the negative frequency component. Then the negative frequency component of the circularly polarized photon with helicity $\zeta = \pm 1$ can be expressed as (after stripping off delta functions)

$$\begin{aligned} A_{x,\mathrm{circular},\zeta} &= \frac{A_0}{2}(-\cos\theta_\mathrm{p}\sin\phi_\mathrm{p} - \zeta i\cos\phi_\mathrm{p}), \\ A_{y,\mathrm{circular},\zeta} &= \frac{A_0}{2}(+\cos\theta_\mathrm{p}\cos\phi_\mathrm{p} - \zeta i\sin\phi_\mathrm{p}). \end{aligned} \tag{17}$$

Various scattering processes can contribute to the momentum relaxation of charge carriers. In this paper, just for simplicity, we consider only the elastic scattering by random potentials. The interaction of TMDCs with random potential $V(\mathbf{x})$ (in position space) in second quantization is given by (we will suppress spin and orbital indices for a moment)

$$\mathsf{H}_\mathrm{ran} = \int d^2\mathbf{x}\, V(\mathbf{x})\hat{\mathsf{c}}^\dagger(\mathbf{x})\hat{\mathsf{c}}(\mathbf{x}). \tag{18}$$

Next decompose the electron operator into each valley:

$$\hat{\mathsf{c}}(\mathbf{x}) \approx e^{iK\cdot\mathbf{x}}\hat{\mathsf{c}}_+(\mathbf{x}) + e^{i(-K)\cdot\mathbf{x}}\hat{\mathsf{c}}_-(\mathbf{x}). \tag{19}$$

Then, Eq. (18) becomes

$$\begin{aligned} \mathsf{H}_\mathrm{ran} = \int d^2\mathbf{x}\Big[& V(\mathbf{x})\sum_{l=\pm}\hat{\mathsf{c}}_l^\dagger(\mathbf{x})\hat{\mathsf{c}}_l(\mathbf{x}) \\ & + V(\mathbf{x})\, e^{2iK\cdot\mathbf{x}}\hat{\mathsf{c}}_-^\dagger(\mathbf{x})\hat{\mathsf{c}}_+^\dagger(\mathbf{x}) + \mathrm{H.c.}\Big]. \end{aligned} \tag{20}$$

Thus the intervalley scattering potential [the second term of Eq. (20)] becomes generically complex, while the intravalley scattering potential [the first term of Eq. (20)] is real. These potentials can be combined in the form of a 2×2 matrix in valley space (and identity matrix in other spaces):

$$\begin{aligned} \hat{V}(\mathbf{x}) &= \begin{pmatrix} v_a(\mathbf{x}) & v_r(\mathbf{x}) \\ v_r^*(\mathbf{x}) & v_a(\mathbf{x}) \end{pmatrix}, \\ \mathsf{H}_\mathrm{ran} &= \int d^2\mathbf{x} \sum_{l,m=\pm}\hat{\mathsf{c}}_l^\dagger(\mathbf{x})\hat{V}_{lm}(\mathbf{x})\hat{\mathsf{c}}_m(\mathbf{x}), \end{aligned} \tag{21}$$

where $v_a(\mathbf{x})$ and $v_r(\mathbf{x})$ denote the intravalley scattering potential and the intervalley scattering potential, respectively.

The probability distribution of the random potential is characterized by the first and the second cumulants of the following form:

$$\begin{aligned} &\langle v_a(\mathbf{x})v_a(\mathbf{x}')\rangle = W_a(|\mathbf{x}-\mathbf{x}'|),\ \langle v_r(\mathbf{x})v_r^*(\mathbf{x}')\rangle = W_r(|\mathbf{x}-\mathbf{x}'|), \\ &\langle v_a(\mathbf{x})v_r^*(\mathbf{x}')\rangle = \langle v_a(\mathbf{x})v_r(\mathbf{x}')\rangle = 0,\ \langle v_a(\mathbf{x})\rangle = \langle v_r(\mathbf{x})\rangle = 0, \end{aligned} \tag{22}$$

and all other higher order moments of probability distribution are assumed to vanish. In this paper we will consider the second cumulant of white-noise type $W_{a,r}(|\mathbf{x}-\mathbf{x}'|) = w_{a,r}\delta(|\mathbf{x}-\mathbf{x}'|)$, for simplicity.

Now, the total Hamiltonian in the second quantized form is given by (spin, valley, and orbital indices of electron operators $\hat{\mathsf{c}},\hat{\mathsf{c}}^\dagger$ are suppressed)

$$\mathsf{H}_\mathrm{total} = \sum_{\mathbf{k}}\hat{\mathsf{c}}_\mathbf{k}^\dagger[\hat{\mathsf{h}}_{(0)} + \hat{\mathsf{h}}_{\mathrm{e-ph}}]\hat{\mathsf{c}}_\mathbf{k} + \mathsf{H}_\mathrm{tilt} + \mathsf{H}_\mathrm{ran}, \tag{23}$$

where the second quantized band-tilting Hamiltonian H_tilt is given by

$$\mathsf{H}_\mathrm{tilt} = \int d^2\mathbf{x}\,\hat{\mathsf{c}}^\dagger(\mathbf{x})\big(e\vec{E}_\mathrm{tilt}\cdot\mathbf{x}\big)\hat{\mathsf{c}}(\mathbf{x}). \tag{24}$$

The second quantized current operator is [see Eq. (8)]

$$\mathbf{J} = (-e)\sum_{\mathbf{k}}\hat{\mathsf{c}}_\mathbf{k}^\dagger\frac{\partial\hat{\mathsf{h}}_{(0)}}{\partial\mathbf{k}}\hat{\mathsf{c}}_\mathbf{k}. \tag{25}$$

Our task is to compute the expectation value of the current operator Eq. (25) in the second order of $\hat{\mathsf{h}}_{\mathrm{e-ph}}$ (the nonlinear response).

From the viewpoint of perturbation theory in quantum field theory, the expectation value of current $\langle\mathbf{J}(t)\rangle$ is the so-called *less* Green's function $G^<$ [21], which cannot be computed directly in the standard zero-temperature perturbation theory or the finite-temperature imaginary-time perturbation theory [21]. This is because $T=0$ perturbation theory and imaginary-time perturbation theory are based on the time-ordered Green's function, while the "less" Green's function is not time ordered. We will employ the KS formalism which can incorporate the "less" Green's function (and other related Green's functions) in a systematic way.

C. Keldysh-Schwinger formalism

In this section we formulate the problem of the calculation of photocurrent $\langle\mathbf{J}(t)\rangle$ in KS functional integral framework. The general Keldysh-Schwinger formalism is very well expounded in the literature [15–17], and in this section we will only give a very brief summary of the formalism mainly to establish notations. Also, the coherent state functional integral quantization method will be used [15,22] for actual computations.

The key element of KS formalism is the concept of the *closed time contour* which consists of a forward and backward branch. Quantum operators are to be ordered on this contour, and the Green's functions of these contour-ordered operators can be computed using the method of the standard quantum field theory, such as the Feynman diagram method [15,16]. For example, in the computation of the expectation value of the current operator Eq. (25), the creation operator should be placed on backward branches, while the destruction operator is to be placed on the forward branch. This means that the

"less" Green's function $G^<(t,t')$ is naturally incorporated in the KS formalism.

The coherent state is an eigenstate of the destruction operator, so that

$$\hat{\mathsf{c}}|\psi_\pm\rangle = \psi_\pm|\psi_\pm\rangle, \quad \langle\psi_\pm|\hat{\mathsf{c}}^\dagger = \langle\psi_\pm|\psi_\pm^*, \tag{26}$$

where $+$ $(-)$ designates the forward (backward) branch of the KS contour. If $\hat{\mathsf{c}}$ is a fermion operator, its eigenvalue $\psi_\pm$ is the anticommuting Grassmann number. Suppose $\widehat{C}$ is a general operator which is a function of (normal ordered) $\hat{\mathsf{c}}^\dagger,\hat{\mathsf{c}}$ and that it is to be placed on the forward branch. Then in the KS functional integral formulation we have a map:

$$\widehat{C}(\hat{\mathsf{c}}^\dagger,\hat{\mathsf{c}})|_{\text{forward branch}} \to C(\psi_+^*,\psi_+). \tag{27}$$

In an entirely similar way,

$$\widehat{C}(\hat{\mathsf{c}}^\dagger,\hat{\mathsf{c}})|_{\text{backward branch}} \to C(\psi_-^*,\psi_-). \tag{28}$$

In practical calculations, the following combinations (for fermions only) turn out to be more convenient [15,16] (momentum labels are reinstated):

$$\begin{aligned}\psi_{1/2}(\mathbf{k},t) &= \frac{1}{\sqrt{2}}[\psi_+(\mathbf{k},t) \pm \psi_-(\mathbf{k},t)],\\ \bar{\psi}_{1/2}(\mathbf{k},t) &= \frac{1}{\sqrt{2}}[\psi_+^*(\mathbf{k},t) \mp \psi_-^*(\mathbf{k},t)].\end{aligned} \tag{29}$$

The new indices 1, 2 will be called Keldysh indices. Then KS Green's function takes the following form [15,16]:

$$(-i)\langle\psi_a(t)\bar{\psi}_b(t')\rangle = \begin{pmatrix} G^{\mathsf{R}}(t,t') & G^{\mathsf{K}}(t,t') \\ 0 & G^{\mathsf{A}}(t,t') \end{pmatrix}_{ab}, \tag{30}$$

where a,b are Keldysh indices. $G^{\mathsf{R}}(t,t'),G^{\mathsf{A}}(t,t')$ is the retarded Green's function and the advanced Green's function, respectively. The advanced Green's function is the Hermitian conjugate of the retarded Green's function. In energy-momentum space,

$$G^{\mathsf{A}}(\epsilon,\mathbf{k}) = [G^{\mathsf{R}}(\epsilon,\mathbf{k})]^\dagger. \tag{31}$$

At thermal equilibrium the Keldysh component of the fermion Green's function G^{K} is given by the fluctuation-dissipation theorem:

$$G^{\mathsf{K}}(\epsilon,\mathbf{k}) = \tanh\frac{\epsilon}{2k_BT}[G^{\mathsf{R}}(\epsilon,\mathbf{k}) - G^{\mathsf{A}}(\epsilon,\mathbf{k})], \tag{32}$$

where ϵ is the energy measured from the chemical potential.

Now we can map the operators in Sec. II B into KS functional integral form. The electric current operator Eq. (25) maps to

$$\mathbf{J}(t) = (-e)\sum_{\mathbf{k}} \bar{\Psi}_{\mathbf{k}}(t)\,\mathsf{E}_< \otimes \frac{\partial\hat{\mathsf{h}}_{(0)}}{\partial\mathbf{k}}\,\Psi_{\mathbf{k}}(t), \tag{33}$$

where Ψ is a multicomponent spinor in Keldysh (1,2) and spin/valley/orbital space (collectively denoted by a),

$$\Psi = (\psi_{1\mathsf{a}},\psi_{2\mathsf{a}})^{\mathrm{t}}, \tag{34}$$

where "t" is a matrix transpose, and

$$\mathsf{E}_< = \frac{1}{2}\begin{pmatrix} -1 & -1 \\ 1 & 1 \end{pmatrix}. \tag{35}$$

The photon vector potential and the random potentials are classical [15], meaning that they are identical in both the forward and backward branches. For these classical potentials, the Keldysh matrix (such as $\mathsf{E}_<$ above) of the interaction becomes a 2×2 identity matrix in Keldysh space [15].

The expectation value of the current operator in KS functional integral formulation can be represented as

$$\langle\mathbf{J}(t)\rangle = \int P[V_{\text{ran}}]\int D[\bar{\Psi},\Psi]\,e^{iS_{\text{total}}}\mathbf{J}(t), \tag{36}$$

where $\int P[V_{\text{ran}}]$ indicates the average over the probability distribution of disorder which gives the cumulants Eq. (22). S_{total} is the action corresponding the Hamiltonian Eq. (23). To obtain the photocurrent we need to expand Eq. (36) with respect to the electron-photon interaction term to the second order (as discussed in Sec. II A).

For perturbation theory, we need the bare (noninteracting) retarded and advanced Green's functions. These can be obtained by the following the 8×8 matrix inversion (μ is chemical potential, and I_8 is the 8×8 identity matrix):

$$G_0^{\mathsf{R/A}}(\epsilon,\mathbf{k}) = [(\epsilon+\mu\pm i0^+)\mathrm{I}_8 - \mathsf{h}_{(0)}]^{-1}, \tag{37}$$

where 0^+ is an infinitesimally small positive quantity. Noting that the matrices in Eq. (37) are diagonal in spin and valley space, the full Green's function can be written as a direct sum in each $s=\pm1,\eta=\pm1$ block. The explicit form of the Green's function in the s,η block is given by

$$\begin{aligned}G_0^{\mathsf{R/A},s\eta}(\epsilon,\mathbf{k}) &= \frac{\widehat{\mathsf{D}}}{[\epsilon+\mu\pm i0^+ - E_{\mathsf{c}}][\epsilon+\mu\pm i0^+ - E_{\mathsf{v},s\eta}]},\\ \widehat{\mathsf{D}} &= \begin{pmatrix} \epsilon+\mu+\frac{\Delta}{2}-s\eta\lambda & v\eta k_x - ivk_y \\ v\eta k_x + ivk_y & \epsilon+\mu-\frac{\Delta}{2}\end{pmatrix}.\end{aligned} \tag{38}$$

$E_{\mathsf{c}} = E_{\mathsf{c}}(\mathbf{k})$ and $E_{\mathsf{v},s\eta} = E_{\mathsf{v},s\eta}(\mathbf{k})$ are the conduction band and the valence band energies with the approximation taken in Eq. (5).

The bare Keldysh component Green's function can be obtained from Eq. (32). The full bare KS Green's function is given by

$$\widehat{G}_0(\epsilon,\mathbf{k}) = \begin{pmatrix} G_0^{\mathsf{R}}(\epsilon,\mathbf{k}) & G_0^{\mathsf{K}}(\epsilon,\mathbf{k}) \\ 0 & G_0^{\mathsf{A}}(\epsilon,\mathbf{k})\end{pmatrix}, \tag{39}$$

which is a 16×16 matrix in Keldysh-spin-valley-orbital space.

III. CALCULATION

We first compute the self-energy which incorporates elastic random potential scattering, then construct the renormalized Green's functions via the Dyson equation. These renormalized Green's functions are used in the computation of the photocurrent, and the imaginary part of the self-energy plays the role of momentum relaxation time.

A. Calculation of self-energy

The elastic scatterings by random potential provide the momentum relaxation mechanism for the photocurrent. Such momentum relaxation can be described in terms of the self-energy $\widehat{\Sigma}(\epsilon,\mathbf{k})$ of Green's functions, and the renormalized

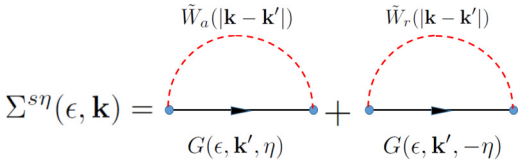

FIG. 1. The lowest order Feynman diagrams contributing to self-energy. The solid line indicates the bare Green's function $\widehat{G}_0(\epsilon,\mathbf{k}',\eta)$ with chirality η, and the dotted line indicates the random potential average. $\tilde{W}_{r,a}(|\mathbf{k}-\mathbf{k}'|)$ are the Fourier transform of the second cumulants.

Green's function can be expressed as (Dyson equation)

$$\widehat{G}(\epsilon,\mathbf{k}) = \left[\widehat{G}_0^{-1}(\epsilon,\mathbf{k}) - \widehat{\Sigma}(\epsilon,\mathbf{k})\right]^{-1}. \tag{40}$$

Since the Keldysh matrix of classical random potential is identity, the Keldysh matrix structure of self-energy is identical with that of the bare Green's function Eq. (39). Therefore, we need to compute the self-energy only for the retarded Green's function since the advanced and the Keldysh component can be obtained by Hermitian conjugation and by the fluctuation-dissipation theorem [see Eqs. (31) and (32)]. The Feynman diagrams for the self-energy $\widehat{\Sigma}(\epsilon,\mathbf{k})$ in the lowest order Born approximation are depicted in Fig. 1.

From Feynman rules of the KS formalism, we obtain the following retarded self-energy in the (s,η) block:

$$\Sigma^{\mathsf{R},s\eta}(\epsilon,\mathbf{k}) = \int \frac{d^2\mathbf{k}'}{(2\pi)^2}\left[\widehat{G}_0^{\mathsf{R},s\eta}(\epsilon,\mathbf{k}')\tilde{W}_a(|\mathbf{k}-\mathbf{k}'|) + \widehat{G}_0^{\mathsf{R},s(-\eta)}(\epsilon,\mathbf{k}')\tilde{W}_r(|\mathbf{k}-\mathbf{k}'|)\right], \tag{41}$$

where $\widehat{G}_0^{\mathsf{R},s\eta}(\epsilon,\mathbf{k}')$ is the bare Green's function Eq. (38). $\tilde{W}_{a,r}(|\mathbf{k}-\mathbf{k}'|)$ are the Fourier transform of the second cumulants of the random potential Eq. (22). Note that in the second term of Eq. (41) the Green's function with the opposite chirality $-\eta$ appears due to the intervalley scattering.

The real part of the self-energy can be absorbed into the chemical potential and renormalization of velocity v, while the momentum relaxation process is captured by the imaginary part of the self-energy. We will assume that the real part of the self-energy has already been incorporated into the bare Green's function, and will focus on the imaginary part. Since we are assuming the white-noise type random potential distribution, $\tilde{W}_{a,r}(|\mathbf{k}-\mathbf{k}'|)$ are constants:

$$\tilde{W}_a(|\mathbf{k}-\mathbf{k}'|) = w_a, \quad \tilde{W}_r(|\mathbf{k}-\mathbf{k}'|) = w_r. \tag{42}$$

The angle integral of Eq. (41) is easily performed, and the integral over $|\mathbf{k}|$ for the imaginary part can be done using $\mathrm{Im}\frac{1}{x+i0^+} = -\pi\delta(x)$. The leading contribution to the imaginary part turns out to be independent of spin, valley, and orbital quantum number,

$$\mathrm{Im}\Sigma^{\mathsf{R},s\eta}(\epsilon,\mathbf{k}) \approx -\frac{1}{4}\frac{\Delta(w_a+w_r)}{v^2}\mathrm{I}_2^\sigma \equiv -\tau^{-1}\mathrm{I}_2^\sigma, \tag{43}$$

where τ is the momentum relaxation time scale. Recalling the bare Green's function Eq. (37), the renormalized Green's function incorporating the self-energy by random potential scattering becomes

$$G^{\mathsf{R/A}}(\epsilon,\mathbf{k}) = [(\epsilon+\mu\pm i\tau^{-1})\mathrm{I}_8 - \mathsf{h}_{(0)}]^{-1}. \tag{44}$$

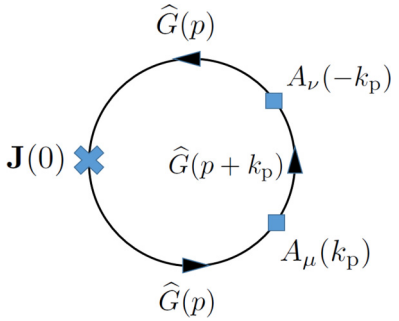

FIG. 2. The Feynman diagram for photocurrent without band-tilting perturbation. The solid lines are for the renormalized Green's function Eq. (40). The cross indicates the insertion of current density operator at zero energy and momentum. The filled square denotes the electron-photon interaction vertex.

In terms of the 2×2 matrix Green's function $G^{\mathsf{R/A},s\eta}(\epsilon,\mathbf{k})$ in the s,η block [see Eq. (38)], the renormalized Green's function can be obtained from the bare Green's function by the substitution

$$\epsilon \pm i0^+ \to \epsilon \pm i\tau^{-1}. \tag{45}$$

Now we are ready to compute the photocurrent.

B. Calculation of photocurrent

We are looking for a photocurrent uniform in space and constant in time. Therefore, we must compute the expectation value of the current operator Eq. (36) with zero energy and momentum in the second order of electron-photon interaction.

Let us start with the case of the zeroth order in the band-tilting perturbation. The corresponding Feynman diagram is depicted in Fig. 2.

The straightforward application of Feynman rules in the KS formalism yields the following result for the photocurrent; recall that the current vertex matrix $\widehat{\mathsf{M}}_\mu$ is defined by Eq. (9) and the Keldysh matrix $\mathsf{E}_<$ is defined in Eq. (35); I_2^k is the 2×2 identity matrix in Keldysh space, and $i,\mu,\nu = x,y$ (here μ is not to be confused with chemical potential):

$$\langle J^i(q=0)\rangle = \frac{(-i)(-e)^3v^3}{c^2}\sum_{\mu,\nu=x,y}\int (dk)A^\mu(k_\mathrm{p})A^\nu(-k_\mathrm{p}) \times \mathrm{Tr}[\mathsf{E}_<\otimes\widehat{\mathsf{M}}_i\,\widehat{G}(k)\,\mathrm{I}_2^\mathsf{k} \otimes \widehat{\mathsf{M}}_\mu\widehat{G}(k+k_\mathrm{p})\mathrm{I}_2^\mathsf{k}\otimes\widehat{\mathsf{M}}_\nu\,\widehat{G}(k)], \tag{46}$$

where k,k_p are the energy-momentum vectors of the electron and photon, respectively:

$$k = (\epsilon,\mathbf{k}),\ \ k_p = (\omega_\mathrm{p},\mathbf{k}_\mathrm{p}),\ \ (dk) = \int\frac{d^2\mathbf{k}d\epsilon}{(2\pi)^3}. \tag{47}$$

The trace Tr is over both Keldysh and spin/valley/orbital indices. $\widehat{G}(k)$ is the renormalized Keldysh Green's function (namely with momentum relaxation processes included):

$$\widehat{G}(\epsilon,\mathbf{k}) = \begin{pmatrix} G^\mathsf{R}(\epsilon,\mathbf{k}) & G^\mathsf{K}(\epsilon,\mathbf{k}) \\ 0 & G^\mathsf{A}(\epsilon,\mathbf{k})\end{pmatrix}, \tag{48}$$

where the renormalized retarded and advanced Green's function are given by Eq. (44). As explained just below Eq. (16),

the negative frequency component has been selected. After carrying out the partial trace over the Keldysh index, we arrive at (now tr is the trace over spin/valley/orbital space)

$$\langle J^i(0)\rangle = \frac{(-i)(-e)^3 v^3}{2c^2}\int (dk)\tilde{A}^{\mu}\tilde{A}^{\nu *}\mathrm{tr}[-\widehat{\mathsf{M}}_i G^{\mathsf{R}}(k)\widehat{\mathsf{M}}_{\mu}G^{\mathsf{R}}(k+k_{\mathrm{p}})\widehat{\mathsf{M}}_{\nu}G^{\mathsf{R}}(k) + \widehat{\mathsf{M}}_i G^{\mathsf{A}}(k)\widehat{\mathsf{M}}_{\mu}G^{\mathsf{A}}(k+k_{\mathrm{p}})\widehat{\mathsf{M}}_{\nu}G^{\mathsf{A}}(k)$$
$$+ \widehat{\mathsf{M}}_i G^{\mathsf{R}}(k)\widehat{\mathsf{M}}_{\mu}G^{\mathsf{R}}(k+k_{\mathrm{p}})\widehat{\mathsf{M}}_{\nu}G^{\mathsf{K}}(k) + \widehat{\mathsf{M}}_i G^{\mathsf{R}}(k)\widehat{\mathsf{M}}_{\mu}G^{\mathsf{K}}(k+k_{\mathrm{p}})\widehat{\mathsf{M}}_{\nu}G^{\mathsf{A}}(k) + \widehat{\mathsf{M}}_i G^{\mathsf{K}}(k)\widehat{\mathsf{M}}_{\mu}G^{\mathsf{A}}(k+k_{\mathrm{p}})\widehat{\mathsf{M}}_{\nu}G^{\mathsf{A}}(k)]. \quad (49)$$

The first two terms in the brackets of Eq. (49) involving only the retarded and the advanced Green's functions vanish upon the ϵ integral due to analytic properties originating from causality (e.g., a retarded Green's function is analytic in the upper half plane of complex ϵ plane). Then the remaining three terms in the brackets of Eq. (49) can be reorganized in the following way, employing the fluctuation-dissipation theorem relation Eq. (32):

$$\langle J^i\rangle = \frac{(-i)(-e)^3 v^3}{2c^2}\int (dk)\,\tilde{A}^{\mu}\tilde{A}^{\nu *}\Bigg[\tanh\frac{\epsilon}{2k_BT}\{\mathrm{tr}[\widehat{\mathsf{M}}_i G^{\mathsf{R}}(k)\widehat{\mathsf{M}}_{\mu}G^{\mathsf{R}}(k+k_{\mathrm{p}})\widehat{\mathsf{M}}_{\nu}G^{\mathsf{R}}(k)]$$
$$- \mathrm{tr}[\widehat{\mathsf{M}}_i G^{\mathsf{A}}(k)\widehat{\mathsf{M}}_{\mu}G^{\mathsf{A}}(k+k_{\mathrm{p}})\widehat{\mathsf{M}}_{\nu}G^{\mathsf{A}}(k)]\} + \left(\tanh\frac{\epsilon}{2k_BT} - \tanh\frac{\epsilon+\omega_{\mathrm{p}}}{2k_BT}\right)$$
$$\times\{\mathrm{tr}[\widehat{\mathsf{M}}_i G^{\mathsf{R}}(k)\widehat{\mathsf{M}}_{\mu}G^{\mathsf{A}}(k+k_{\mathrm{p}})\widehat{\mathsf{M}}_{\nu}G^{\mathsf{A}}(k)] - \mathrm{tr}[\widehat{\mathsf{M}}_i G^{\mathsf{R}}(k)\widehat{\mathsf{M}}_{\mu}G^{\mathsf{R}}(k+k_{\mathrm{p}})\widehat{\mathsf{M}}_{\nu}G^{\mathsf{A}}(k)]\}\Bigg]. \quad (50)$$

Using the conjugation relation Eq. (31) it is easily seen the photocurrent $\langle J^i\rangle$ is explicitly real (as it should be).

Now it is easily found that the angle integration gives a vanishing result for the photocurrent. This is because only the odd number of products of electron momentum components $\mathbf{k}$ survives after Pauli matrix algebra $\mathrm{tr}(\hat{\sigma}_i\hat{\sigma}_j) = 2\delta_{ij}$, $\hat{\sigma}_i\hat{\sigma}_j = \mathrm{I}_2^{\sigma}\delta_{ij} + i\epsilon^{ijk}\hat{\sigma}_k$ and the summation over the valley quantum number $\eta = \pm 1$. Another way of understanding this result is as follows: after the angle integral, the quantities in brackets must be invariant tensors with three indices i,μ,ν, for there is no vectorial quantity in the brackets (note that the photon momentum $\mathbf{k}_{\mathrm{p}}$ is neglected). Then, the only possible invariant tensor is $\epsilon_{i\mu\nu}$, and it gives a vanishing result because the indices i,μ,ν can take only two possible values x and y. This vanishing result is very similar to that of the photocurrent of the surface states of a 3-dimensional topological insulator: in the absence of external field or symmetry breaking, the photocurrent vanishes even for arbitrary photon incidence angle just like our case [23,24]. To obtain a nonvanishing photocurrent in the case of a topological insulator, additional perturbations are necessary such as external magnetic field, trigonal distortion, Zeeman coupling to photon vector potential [23,24], or photon-drag effect [25,26]. For reviews on the photogalvanic effect and photon drag effect of quantum wells and graphene, see Refs. [27,28].

Therefore we can see that the perturbation by the band-tilting Hamiltonian Eq. (24) is absolutely essential in obtaining nonvanishing photocurrent. Let us include its effect in the first order. It will turn out that the first-order contribution yields a nonvanishing photocurrent. From the form of Eq. (24) we can see the band-tilting term will insert the interaction vertex (in Hamiltonian form and in momentum space)

$$\frac{i}{2}e\vec{E}_{\mathrm{tilt}}\cdot\frac{\overleftrightarrow{\partial}}{\partial\mathbf{k}}, \quad (51)$$

where $\overleftrightarrow{\partial}$ indicates that the derivative acts on two operators of Eq. (24). The band-tilting interaction vertex can be inserted in three ways as shown in Fig. 3.

The application of Feynman rules shows that the insertion of the band-tilting interaction vertex is equivalent to the following replacement of the fermion Green's function:

$$G^{\mathsf{R/A}} \to \frac{1}{2}e\vec{E}_{\mathrm{tilt}}\cdot\left(G^{\mathsf{R/A}}\frac{\partial G^{\mathsf{R/A}}}{\partial\mathbf{k}} + \frac{\partial G^{\mathsf{R/A}}}{\partial\mathbf{k}}G^{\mathsf{R/A}}\right). \quad (52)$$

Explicit calculation shows that the right-hand side of Eq. (52) (in s,η subspace and recall $\vec{\ell}_t$ is the unit vector along $\vec{E}_{\mathrm{tilt}}$) becomes

$$\delta G^{\mathsf{R/A},s\eta}(\epsilon,\mathbf{k}) = \frac{(e|\vec{E}_{\mathrm{tilt}}|v^2\hbar^2\mathbf{k}\cdot\vec{\ell}_t)}{[\epsilon+\mu\pm i\tau^{-1}-E_{\mathsf{c}}(\mathbf{k})]^2} \times\frac{1}{[\epsilon+\mu\pm i\tau^{-1}-E_{\mathsf{v},s\eta}(\mathbf{k})]^2}\mathrm{I}_2^{\sigma}. \quad (53)$$

From now on μ is set to 0, and we will neglect the spin-orbit splitting term λ of valence band energy which gives a subleading contribution to the photocurrent.

Let us go back to Eq. (50). We observe that the terms proportional to $\tanh\frac{\epsilon}{2k_BT}$ give a smaller contribution than the ones proportional to $(\tanh\frac{\epsilon}{2k_BT} - \tanh\frac{\epsilon+\omega_{\mathrm{p}}}{2k_BT})$. This is because the leading contribution from the terms proportional to $\tanh\frac{\epsilon}{2k_BT}$, after $\mathbf{k}$ integrals, is independent of ϵ, so that it

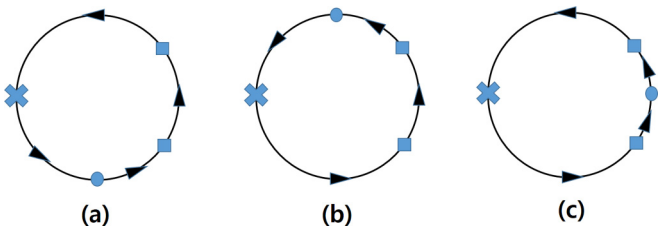

FIG. 3. The Feynman diagrams for photocurrent with band-tilting interaction vertex inserted. The band-tilting interaction vertex is depicted by filled circles in the figure. Other notations are identical with those of Fig. 2. The leading contributions to the helicity-independent photocurrent come from diagrams (a) and (b), while the helicity-dependent photocurrent stems from diagram (c).

vanishes upon the ϵ integral since $\tanh\frac{\epsilon}{2k_BT}$ is an odd function of ϵ.

Next consider the zero-temperature limit (see Sec. II A) of the second term of Eq. (50). In this limit, the factor $(\tanh\frac{\epsilon}{2k_BT}-\tanh\frac{\epsilon+\omega_p}{2k_BT})$ becomes a bump function: -2 in the interval $-\omega_p<\epsilon<0$ and zero, otherwise. This limit simplifies the integral over ϵ considerably. Note that the dependence on the chemical potential essentially stems from these distribution functions $\tanh\frac{\epsilon}{2k_BT}$ and $\tanh\frac{\epsilon+\omega_p}{2k_BT}$ because the energy ϵ is measured from the chemical potential.

The essential part of diagram (a) of Fig. 3 is given by

$$\mathrm{tr}[\widehat{\mathsf{M}}_i\delta G^{\mathsf{R}}(k)\widehat{\mathsf{M}}_\mu G^{\mathsf{A}}(k+k_p)\widehat{\mathsf{M}}_\nu G^{\mathsf{A}}(k)], \tag{54}$$

along with the similar expressions for diagrams (b) and (c). Now we have to calculate the momentum and the energy integral of Eq. (54). Rather than displaying the full details of calculations, we just point out the key steps (assuming the zero chemical potential of the intrinsic case).

(1) Carry out traces over spin/valley/orbital spaces. The traces will decompose into $s=\pm1,\eta=\pm1$ blocks. Then do the angle integral. Now the angle integral does not vanish owing to the additional angle factor coming from $\mathbf{k}\cdot\vec{\ell}_t$ [see Eq. (53)].

(2) Due the the occupation number factor $(\tanh\frac{\epsilon}{2k_BT}-\tanh\frac{\epsilon+\omega_p}{2k_BT})$ the energy takes a negative value in the range $[-\omega_p,0]$. In this energy range, the valence band components of Eqs. (38) and (53), namely $[\epsilon\pm i\tau^{-1}-E_v(\mathbf{k})]^{-1}$, become singular at $k_*^2=(\Delta/v^2)(-\Delta/2-\epsilon)$. Then, carry out the integral over k^2 using the Laplace method of the asymptotic integral, and neglect the subleading terms in accordance with the relative energy scales.

(3) Then the resulting integral [for diagrams (a) and (b); diagram (c) can be computed similarly] is proportional to

$$\left(-\frac{\Delta}{2}-\epsilon\right)\frac{\Delta^2\tau}{v^4}\left[\frac{1}{(2\epsilon)^3}\,\frac{1}{2\epsilon+\omega_p-i/\tau}\,\frac{1}{\omega_p}\right]. \tag{55}$$

The factor $(2\epsilon+\omega_p-i/\tau)^{-1}$ is, effectively, the electron propagator in the conduction band. Since this factor is peaked at $2\epsilon_*=-\omega_p$, the remaining ϵ integrals can be done again by using the Laplace method.

(4) After the ϵ integral, we obtain the leading contribution to the integral:

$$\frac{(-e)^4v^2|\vec{E}_{\mathrm{tilt}}|\tau}{c^2}\,\frac{(\omega_p-\Delta)\Delta^2}{\omega_p^4}, \tag{56}$$

apart from the polarization factors coming from $\tilde{A}_\mu,\tilde{A}_\nu^*$ of Eq. (50). We have neglected spin-orbit splitting λ compared to photon energy ω_p.

(5) Multiplying the appropriate polarization factors, we can obtain the final results, which are presented in the next section.

IV. RESULTS AND DISCUSSION

The experimental data of [13] have been presented in the form of the normalized photocurrent:

$$\mathbf{J}_{\mathrm{normalized}}=\frac{\mathbf{J}}{(|\vec{S}_{\mathrm{Poynting}}|\times\text{Sample Area})}, \tag{57}$$

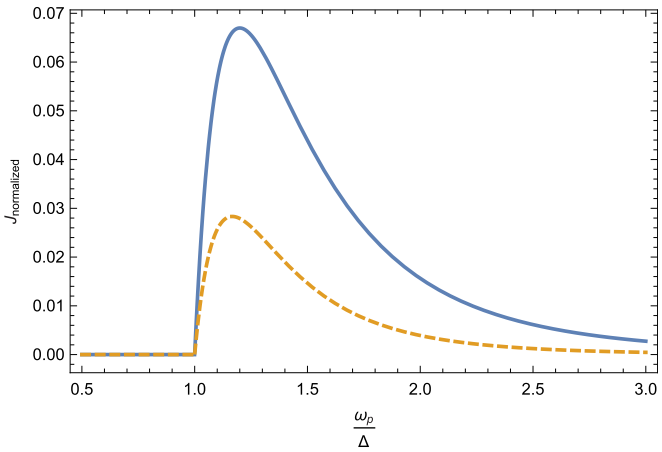

FIG. 4. The photon energy (in units of the band gap) dependence of the normalized photocurrent $\mathbf{J}_{\mathrm{normalized}}$ (in arbitrary units). The thick line and dashed line is for the helicity-independent and the helicity-dependent photocurrent, respectively. The helicity-dependent photocurrent has been magnified for visibility.

where $|\vec{S}_{\mathrm{Poynting}}|$ is the laser intensity (the magnitude of Poynting vector). In terms of the amplitude A_0 of the photon vector potential, the laser intensity is given by

$$|\vec{S}_{\mathrm{Poynting}}|=\frac{1}{8\pi}\,\frac{\omega_p^2A_0^2}{c}. \tag{58}$$

We recall that the polarization factors for linear polarization are given by Eqs. (11), (12), and (14). The calculations show that the leading contributions to the photocurrent in the S,P polarization states come from diagrams (a) and (b) of Fig. 3. Diagram (c) gives the subleading contribution.

The normalized photocurrent for the S linearly polarized photon is given by (here, of course, $\omega_p>\Delta$)

$$\mathbf{J}_{S,\mathrm{normalized}}=\tilde{d}_S\,\frac{e^4v^2\tau}{c}|\vec{E}_{\mathrm{tilt}}|\frac{\Delta^2(\omega_p-\Delta)}{\omega_p^6}\times[\hat{\mathbf{x}}\cos(2\phi_p-\phi_t)+\hat{\mathbf{y}}\sin(2\phi_p-\phi_t)], \tag{59}$$

where $\tilde{d}_S$ is a numerical constant of order 1 whose precise value does not concern us here. Recall that ϕ_t is the tilt angle defined just below Eq. (6).

The first notable feature of Eq. (59) is the photon energy dependence $\frac{\omega_p-\Delta}{\omega_p^6}$, which has a broad maximum at $\omega_*=\frac{6}{5}\Delta$. Taking the experimental value of the band gap 2.4 eV the peak is predicted at 2.9 eV, which agrees well with the experimental result. This photon energy dependence of the photocurrent of Fig. 4 is clearly consistent with experimental data (compare with panel (a) in Fig. 2 of Ref. [13]).

Second, we note that there is no polar angle (θ_p) dependence in Eq. (59), which is due to the specific S-polarization geometry Eq. (11). Third, the factor of 2 in the argument $2\phi_p-\phi_t$ indicates that this photocurrent is of the second order in the vector potential of photons.

Next, the photocurrent for the P linearly polarized photon is given by

$$\mathbf{J}_{P,\text{normalized}} = \tilde{d}_P \frac{e^4 v^2 \tau}{c} |\vec{E}_{\text{tilt}}| \frac{\Delta^2(\omega_\text{p} - \Delta)}{\omega_\text{p}^6} \cos^2\theta_\text{p} \times [\hat{\mathbf{x}} \cos(2\phi_\text{p} - \phi_t) + \hat{\mathbf{y}} \sin(2\phi_\text{p} - \phi_t)], \quad (60)$$

where $\tilde{d}_P$ is again a numerical constant of order 1. The crucial difference between the S and P polarization cases is the polar angle dependence of $\cos^2\theta_\text{p}$ of $\mathbf{J}_P$, and other features are identical. We see that the photocurrent becomes maximized for normal incidence $\theta_\text{p} = 0$.

Recall that the polarization factors for circular polarization are given by Eq. (17). The photocurrent for the circularly polarized photon with the helicity $\zeta = \pm 1$ consists of the helicity-independent part and the helicity-dependent part:

$$\mathbf{J}_\text{circular} = \mathbf{J}_\text{ind} + \mathbf{J}_\text{dep}, \quad (61)$$

where ($\tilde{d}_c$,$\tilde{d}_h$ are numerical constants of order 1)

$$\mathbf{J}_{\text{ind,normalized}} = \tilde{d}_c \frac{e^4 v^2 \tau}{c} |\vec{E}_{\text{tilt}}| \frac{\Delta^2(\omega_\text{p} - \Delta)}{\omega_\text{p}^6} \sin^2\theta_\text{p} \times [\hat{\mathbf{x}} \cos(2\phi_\text{p} - \phi_t) + \hat{\mathbf{y}} \sin(2\phi_\text{p} - \phi_t)], \quad (62)$$

$$\mathbf{J}_{\text{dep,normalized}} = \zeta\, \tilde{d}_h \frac{e^4 v^2}{c} |\vec{E}_{\text{tilt}}| \tau^{-1} \frac{\Delta^2(\omega_\text{p} - \Delta)}{\omega_\text{p}^8} \cos\theta_\text{p} \times [\hat{\mathbf{x}} \sin\phi_t + \hat{\mathbf{y}}(-\cos\phi_t)]. \quad (63)$$

All features of the helicity-independent part of photocurrent $\mathbf{J}_\text{ind}$ are identical with those of linearly polarized light except for the polar angle dependence $\sin^2\theta_\text{p}$. As for the helicity-dependent part $\mathbf{J}_\text{dep}$, it reverses its direction for the opposite helicity, and is perpendicular to the tilt direction (the direction of source to drain bias electric field). This is exactly what is expected for the transverse current in the valley Hall effect, namely the charge carriers from different valleys move in the opposite direction perpendicular to the applied electric field [7].

In the case of optical transition of TMDCs for the circularly polarized light, the helicity of the photon is closely tied to the valley quantum number via the optical selection rule (see below), so that the role of the valley quantum number η is reflected in the form of helicity ζ in Eq. (63). We also note the higher power of photon frequency in the denominator ω_p^{-8}, so that its magnitude is considerably smaller than that of the helicity-independent one by a factor of $1/(\tau\omega_\text{p})^2$. Note that we have neglected the spin-orbit interaction in the computation of the photocurrent. If the spin-orbit interaction is not neglected, the valley Hall effect will induce the spin Hall effect, and the spin Hall effect will contribute to the transverse current. In fact, if we compute the expectation value of spin current operator $\mathsf{c}^\dagger \vec{s} \mathsf{c}$ directly, the spin-orbit interaction is expected to give a leading contribution.

Many features of the photocurrent for the circularized polarized photon with helicity $\zeta = \pm 1$ can be understood in terms of the interband optical transition (with normally incident photon) matrix element near the K and K' points (see Eq. (7) of [6]):

$$|\mathcal{P}_\zeta(\mathbf{k})|^2 \propto \left(1 + \zeta\, \eta \frac{\Delta'_{s\eta}}{\sqrt{\Delta'^2_{s\eta} + 4v^2k^2}}\right)^2. \quad (64)$$

Recall that $v = t_\text{hop} a$ and $\Delta'_{s\eta} = \Delta - s\eta\lambda \sim \Delta$. When $vk \ll \Delta$, we have an optical valley selection rule of $\zeta\eta = 1$, which leads to the helicity-dependent photocurrent as discussed above. Evidently, the effect of this optical selection rule will be maximized for normal incidence ($\theta_\text{p} = 0$), and this explains the $\cos\theta_\text{p}$ dependence of Eq. (63).

Nevertheless, the interband optical transition is not limited to the close neighborhood of the K and K' points. The examination of the band structure by first-principles calculations (see Fig. 1 of Ref. [10]) shows that there exists some room in momentum space where the optical valley selection rule $\zeta\eta = 1$ can be relaxed. The contribution from this portion of momentum space results in the helicity-independent contribution to the photocurrent. Clearly, this contribution will become larger when the optical valley selection rule weakens away from the normal incidence (namely large θ_p), and this explains the $\sin^2\theta_\text{p}$ dependence of Eq. (62). However, we would like to mention that the accurate measurement of angle dependence may not be so easy due to the laser focusing in actual experiments. It appears that the angle and polarization dependence of the photocurrent have been unspecified in Ref. [13].

The experimental value of the normalized photocurrent is of the order 10 A/W. By assuming the value of relaxation time $\tau \sim 10^{-8}$ to 10^{-9} s and with the sample size of 1 μm of the experiment [13], our expression for the helicity-independent photocurrent gives the same order of magnitude as that of the experimentally observed photocurrent.

In our calculation, we have neglected the carrier distribution relaxation by inelastic scattering. This can be justified as follows. In the experimental condition (low laser intensity) in which we are interested, the carrier density is so low that the inelastic scattering between charge carriers (electron-electron interaction) can be neglected. Another source of inelastic scattering is the electron-phonon scattering. Again for the case of our interest temperature is very low, so that inelastic scattering by electron-phonon interaction becomes ineffective. Also, technically the full-fledged treatment of inelastic scattering requires many-body interaction and the Boltzmann equation, which is certainly beyond the scope of this paper.

Our computation shows that the nonvanishing photocurrent requires the band-tilting electric field. However, in fact, the C_{3h} trigonal symmetry of the space group at $\mathbf{K}$ can allow nonvanishing photocurrent even for normally incident light [29]. The Hamiltonian of Eq. (2) was derived in the first-order $k \cdot p$ perturbation theory, so that the trigonal distortion terms which appear in the third order of momentum have been neglected. This is why our treatment requires a band-tilting term for a nonvanishing photocurrent. The contribution from trigonal distortion will be too small to have practical significance since all important optical processes occur in the vicinity of the K point.

We note another important mechanism for the polarization-dependent photocurrent of the TMDC coming from the electric dipoles (normal to layer) which are induced when the TMDC is placed on a substrate or heterogeneous stack [30]. This dipole d_z couples to the vector potential of the photon $d_z \dot{A}_z \sigma_z / c$ (see Eq. (7) of Ref. [30]), and this coupling being combined with the Berry curvature effect can give rise to a nonvanishing photocurrent proportional to the electric dipole moment. Recall that in our case the photocurrent is nonvanishing due to the band tilting by the source to drain voltage. So we can say that our band-tilting effect is the counterpart of the electric dipole coupling of Ref. [30]. The experiment of Ref. [13] has been done for the sample in the suspended state to reduce effects coming from the substrate, and this implies that the electric dipole mechanism of Ref. [30] is not directly relevant to Ref. [13]. The polarization dependence of Ref. [30] is very different from ours since this dipole-generated photocurrent is based on different photon coupling [for example compare Eq. (1) of Ref. [30] with our Eqs. (59) and (63)]. However, interestingly, the photon energy dependence (see Eq. (11a) of Ref. [30]) turns out to be similar to ours.

Finally we mention that the photocurrent does not depend on the chemical potential apart from overall numerical constants as long as it stays inside the energy gap. In connection with this we note that, in actual experiment, the gate voltage is adjusted, so that the Fermi level does not reach the conduction or valence band [13].

V. CONCLUSIONS

Photocurrent spectroscopy is a very versatile tool with direct relevance to optoelectronics applications in diverse materials. We also note a recent theoretical work on a new kind of photocurrent, the shift charge and the spin photocurrent, of topological insulators [31]. In view of this, a thorough theoretical understanding of the photocurrent of TMDC material is highly desirable.

The exciton contribution to the photocurrent is clearly important, while the precise theoretical understanding of it is hampered by its apparently strong dependence on the source to drain voltage and/or gate voltage [13] (in other words the unbinding of the electron-hole pair by strong electric field).

In this paper, we instead focused on the direct band-to-band contribution to the photocurrent (obviously, this will be a significant part of the C peak structure of the experiment of [13]). We have computed the photocurrent for arbitrary photon incidence angles and for general photon polarizations based on the microscopic Hamiltonian which incorporates the source to drain bias voltage giving the band tilting. The band-tilting effect turns out to be essential for the nonvanishing photocurrent. Our results are consistent with the experimental data, and furthermore we predict other features such as specific angle dependence and the helicity-dependent component of the photocurrent compatible with the valley Hall effect, which can be readily verified by experiments.

ACKNOWLEDGMENTS

The author is grateful to Hyunsik Cheong and Jae-Ung Lee for very fruitful discussions and critical comments. This research was supported by the Basic Science Research Program through the National Research Foundation of Korea (NRF) funded by the Ministry of Education, Science, and Technology (NRF-2016R 1D 1A 1B03930125).

[1] K. S. Novoselov, D. Jiang, F. Schedin, T. J. Booth, V. V. Khotkevich, S. V. Morozov, and A. K. Geim, Proc. Natl. Acad. Sci. USA **102**, 10451 (2005).
[2] A. K. Geim and I. V. Grigorieva, Nature (London) **499**, 419 (2013).
[3] Y. Yoon, K. Ganapathi, and S. Salahuddin, Nano Lett. **11**, 3768 (2011).
[4] B. Radisavljevic, A. Radenovic, J. Brivio, V. Giacometti, and A. Kis, Nat. Nanotechnol. **6**, 147 (2011).
[5] S. D. Sarma, S. Adam, E. H. Hwang, and E. Rossi, Rev. Mod. Phys. **83**, 407 (2011).
[6] D. Xiao, G. B. Liu, W. Feng, X. Xu, and W. Yao, Phys. Rev. Lett. **108**, 196802 (2012).
[7] X. Xu, W. Yao, D. Xiao, and T. F. Heinz, Nat. Phys. **10**, 343 (2014).
[8] A. Splendiani, L. Sun, Y. Zhang, T. Li, J. Kim, C.-Y. Chim, G. Galii, and F. Wang, Nano Lett. **10**, 1271 (2010).
[9] K. F. Mak, C. Lee, J. Hone, J. Shan, and T. F. Heinz, Phys. Rev. Lett. **105**, 136805 (2010).
[10] D. Y. Qiu, F. H. da Jornada, and S. G. Louie, Phys. Rev. Lett. **111**, 216805 (2013).
[11] A. Ramasubramaniam, Phys. Rev. B **86**, 115409 (2012).
[12] A. Chernikov, T. C. Berkelbach, H. M. Hill, A. Rigosi, Y. Li, O. B. Aslan, D. R. Reichman, M. S. Hybertsen, and T. F. Heinz, Phys. Rev. Lett. **113**, 076802 (2014).
[13] A. R. Klots, A. K. M. Newaz, B. Wang, D. Prasai, H. Krzyzanowska, J. Lin, D. Caudel, N. J. Ghimire, J. Yan, B. L. Ivanov, K. A. Velizhanin, A. Burger, D. G. Mandrus, N. H. Tolk, S. T. Pantelides, and K. I. Bolotin, Sci. Rep. **4**, 6608 (2010).
[14] T. C. Berkelbach, M. S. Hybertsen, and D. R. Reichman, Phys. Rev. B **88**, 045318 (2013).
[15] A. Kamenev, *Field Theory of Non-Equilibrium Systems* (Cambridge University Press, New York, 2011).
[16] J. Rammer, *Quantum Field Theory of Non-Equilibrium States* (Cambridge University Press, New York, 2007).
[17] A. Altland and B. Simons, *Condensed Matter Field Theory*, 2nd ed. (Cambridge University Press, New York, 2010), pp. 602-765.
[18] S. M. Sze, *Physics of Semiconductor Devices* (Wiley-Interscience, New York, 1981).
[19] M. Trescher, B. Sbierski, P. W. Brouwer, and E. J. Bergholtz, Phys. Rev. B **91**, 115135 (2015).
[20] C. K. Chan, N. H. Lindner, G. Refael, and P. A. Lee, Phys. Rev. B **95**, 041104(R) (2017).
[21] G. Mahan, *Many-Particle Physics* (Plenum, New York, 2000).
[22] J. W. Negele and H. Orland, *Quantum Many-Particle Systems* (Addison-Wesley Publishing Company, New York, 1988).
[23] P. Hosur, Phys. Rev. B **83**, 035309 (2011).
[24] A. Junck, G. Refael, and F. von Oppen, Phys. Rev. B **88**, 075144 (2013).
[25] S. Luryi, Phys. Rev. Lett. **58**, 2263 (1987).

[26] H. C. Lee, Physica E (Amsterdam) **79**, 44 (2016).
[27] S. D. Ganichev and L. E. Golub, Phys. Status Solidi B **251**, 1801 (2014).
[28] M. M. Glazov and S. D. Ganichev, Phys. Rep. **535**, 101 (2014).
[29] W. Weber, L. E. Golub, S. N. Danilov, J. Karch, C. Reitmaier, B. Wittmann, V. V. Bel'kov, E. L. Ivchenko, Z. D. Kvon, N. Q. Vinh, A. F. G. van der Meer, B. Murdin, and S. D. Ganichev, Phys. Rev. B **77**, 245304 (2008).
[30] Y. B. Lyanda-Geller, S. Li, and A. V. Andreev, Phys. Rev. B **92**, 241406(R) (2015).
[31] K. W. Kim, T. Morimoto, and N. Nagaosa, Phys. Rev. B **95**, 035134 (2017).